RASĀYAN *J. Chem.*
Vol. 19 | No. 1 | 575-582 | January-March | 2026
ISSN: 0974-1496 | e-ISSN: 0976-0083 | CODEN: RJCABP
http://www.rasayanjournal.com
http://www.rasayanjournal.co.in

NOVEL SYNTHESIS OF S-DOPED ZnO NANOMATERIALS USING SELENICEREUS UNDATUS PEEL EXTRACT FOR ENHANCED UV PHOTOCATALYTIC DEGRADATION OF METHYL ORANGE

A.Kistan[1,✉], P. Mahimairaj[2], S. Mohan[3], R. Jeevalatha[1], and P. Sivakumar[4]
[1]Department of Chemistry, Panimalar Engineering College, Chennai-600123,(Tamil Nadu) India
[2]Department of Mathematics, R.M.K. College of Engineering & Technology, Puduvoyal, Thiruvallur-601206(Tamil Nadu) India
[3]Department of Chemistry, Rajalakshmi Engineering College, Chennai-602105, (Tamil Nadu) India
[4]Department of Mathematics, Panimalar Engineering College, Chennai-600123, (Tamil Nadu) India
✉Corresponding author: vishmikrish@gmail.com

ABSTRACT
This study used Selenicereus Undatus (Dragon fruit) peel extract as a natural reducing and stabilising agent to create sulfur-doped zinc oxide (S-doped ZnO) nanomaterials in a simple and environmentally acceptable manner. In addition to offering a sustainable substitute for traditional chemical synthesis methods, the bio-waste-derived extract improves the process's environmental friendliness. In order to alter ZnO's electrical structure and increase its photocatalytic effectiveness in the presence of UV light, sulfur doping was added. To verify the crystallinity, shape, and optical characteristics of the produced nanomaterials, methods including XRD, UV-Vis spectroscopy, FTIR, and SEM were used. Methyl orange (MO) dye degradation under UV light was used to assess the photocatalytic activity of the S-doped ZnO. The findings showed that the S-doped ZnO displayed.
Keywords: Selenicereus Undatus Peel Extract, Metal Oxide Nanoparticles, Photocatalysis, Methyl Orange.
RASĀYAN *J. Chem.*, Vol. 19, No.1, 2026

INTRODUCTION

Because synthetic dyes are poisonous, non-biodegradable, and persistent in ecosystems, their increasing contamination of water bodies, especially from textile and industrial effluents, poses a major environmental danger. Methyl orange (MO), an anionic azo dye, is one of them that is frequently found in wastewater streams. Physical adsorption, coagulation, and biological degradation are examples of conventional treatment techniques that frequently fail to completely remove such pollutants or may produce secondary waste.[1-3] In this regard, semiconductor-based Photocatalysis has become a viable, economical, and eco-friendly method for breaking down organic pollutants when exposed to light. Most organic dyes cause burns, cancer, dermatitis, digestive and respiratory problems, and mental health problems, among other problems. Green synthesis methods utilising plant-based extracts have attracted a lot of interest recently for the production of nanomaterials. These techniques minimise the usage of dangerous chemicals while also being affordable and sustainable. Fruit peels and other agricultural and food waste are particularly appealing since they are rich in bioactive chemicals that can function as natural doping, stabilising, and reducing agents.

Dragon fruit, or Selenicereus undatus, is one such fruit whose peel includes a range of phytochemicals appropriate for the synthesis of green nanomaterials. In this work, Selenicereus undatus fruit peel (dragon fruit) extract was used to create sulfur-doped ZnO nanoparticles utilising a simple, environmentally friendly co-precipitation process. The structural, morphological, and optical characteristics of the synthesised materials were evaluated by a variety of methods. The breakdown of methyl orange under UV light was used to measure their photocatalytic activity [4–7]. This study demonstrates how fruit waste may

be used to produce high-performance photocatalysts sustainably, helping to both remediate the environment and value trash.

EXPERIMENTAL

Materials

Sigma-Aldrich supplied all other chemicals and reagents, including the 99.4% pure methyl orange-red dye. All of the glassware was acid-washed and thoroughly cleaned with deionised water before being used. Water that had been double-distilled was used in each experiment.

Collection of Selenicereus Undatusfruit and Peel

Selenicereus undatus fruit peels were bought at local vegetable shops in Chennai, Tamil Nadu, South Eastern India, during the post-monsoon season (March 2024).

Fig.-1: Selenicereus Undatus Fruits (SUF) and Peel

Preparation of Selenicereus Undatus Fruit Peel Extract

The peel and pulp of the Selenicereus undatus fruits were separated by gently slicing them (Fig.-1). A Christ Freeze Dryer Alpha 1-4LD plus was used to freeze-dry the extracted pulp for 40–70 hours at –50 °C and 0.040 mbar of pressure. An MRC Knife Mill Cup grinder was then used to turn the dried material into a fine powder. After that, the powdered peel extract was kept at -80 °C till it was examined further.

ZnO-S Nanoparticle Synthesis Using Selenicereus undatus Peel Extract

Zinc nitrate solutions at varying molar concentrations (0.1 M, 0.3 M, and 0.5 M) were combined with 10 mL of Selenicereus undatus peel extract to create sulfur-doped zinc oxide (ZnO-S) nanoparticles. To guarantee that the synthesis process was finished, the reaction mixtures were kept under continuous stirring at 80 °C for three hours. The suspensions were then centrifuged for 30 minutes at 5000 rpm in order to separate the nanoparticles. To get rid of any remaining contaminants, the precipitates were repeatedly rinsed with deionised water. To create S-doped ZnO nanoparticles, the purified material was first dried in a hot air oven at 120 °C for two hours and then calcined at 500 °C for four hours. The hue of the solution progressively changed from light brown during the synthesis.[8-10]

Characterization

An analytical (X' Pert PRO) diffractometer with a Cu-K radiation source (= 0.1541 nm) was used to obtain all powdered X-ray diffraction (XRD) patterns. The UV-Vis absorption spectra were measured using the ELICO SL-159 spectrophotometer. The FT-IR spectra of a dry potassium bromide pellet at room temperature were recorded in the 4000-400 cm-1 area using a 5DX FT-IR spectrometer (spectral resolution 2 cm^{-1}). The field emission-scanning electron microscopy (CARELZEISS) model EV018 was used to examine the material's morphology. An electron microscope (JEOL SM-7600 F, Japan) with a field-emission gun and an acceleration voltage of 200 KV was used to obtain all TEM pictures at room temperature (RT, 298K).

RESULTS AND DISCUSSION

UV Visible Spectroscopy

The optical characteristics of the produced SUF-ZnO-S nanoparticles were examined using UV–visible spectroscopy, as illustrated in Fig.-2. In addition to other absorption peaks at 343 and 346 nm, the

broccoli blossom extract showed a noticeable peak at 361 nm. These spectrum characteristics verify that ZnO-S nanoparticles were successfully formed using the plant-mediated synthesis method.[18-20]

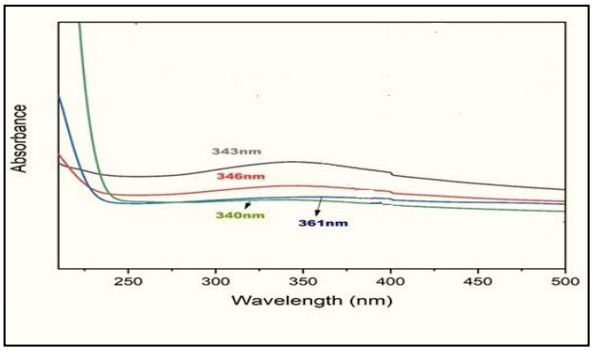

Fig.-2: UV-visible Spectrum for SUF-ZnO-S Nanoparticle

Fourier Transform Infra-Red Spectroscopy (FT-IR)

Figure-3 (A and B) displays the Fourier Transform Infrared (FTIR) spectra of the produced ZnO-S and ZnO-S/Chitosan nanocomposite. The stretching vibrations of surface hydroxyl groups (–OH) and adsorbed water molecules are responsible for the large absorption band at 3432.49 cm^{-1} in the ZnO-S spectra (Fig.-3). The bending vibrations of H–O–H from residual moisture are represented by the peak seen at 1630 cm^{-1}. Zn–O and Zn–S bond vibrations are responsible for the peaks that emerge at 1144, 995, and 918 cm^{-1}, indicating that sulfur was successfully incorporated into the ZnO lattice. The ZnO crystalline structure is indicated by the fingerprint region's distinctive Zn–O stretching vibrations at 665, 615, 496, and 434 cm^{-1}. Figure-3 (A and B) displays the Fourier Transform Infrared (FTIR) spectra of the produced ZnO-S and ZnO-S/Chitosan nanocomposite. The stretching vibrations of surface hydroxyl groups (–OH) and adsorbed water molecules are responsible for the large absorption band at 3432.49 cm^{-1} in the ZnO-S spectra (Fig. 3). The bending vibrations of H–O–H from residual moisture are represented by the peak seen at 1630 cm^{-1}. Zn–O and Zn–S bond vibrations are responsible for the peaks that emerge at 1144, 995, and 918 cm^{-1}, indicating that sulfur was successfully incorporated into the ZnO lattice. The ZnO crystalline structure is indicated by the fingerprint region's distinctive Zn–O stretching vibrations at 665, 615, 496, and 434 cm^{-1}.

Because of the interactions between ZnO and chitosan, the Zn–O stretching vibrations are still present but have been slightly moved to 501 and 435 cm^{-1}. The excellent production of ZnO-S nanoparticles and their successful functionalization with chitosan are confirmed by these FTIR data, which also show how the functional groups of chitosan interact with ZnO to produce a nanocomposite. By enhancing pollutant adsorption and altering ZnO's electronic environment, this interaction is anticipated to increase photocatalytic effectiveness.

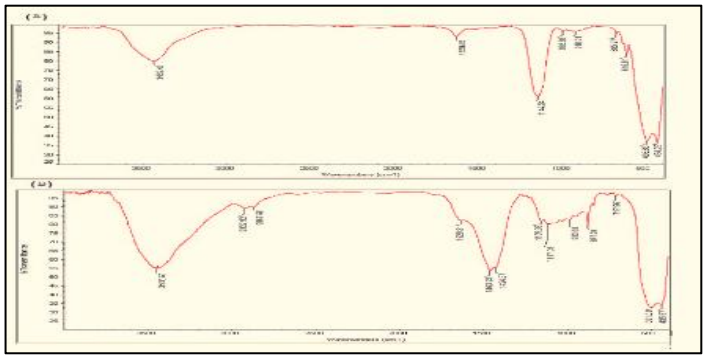

Fig.-3: FT-IR Spectrum for SUF-ZnO-S Nanoparticle

XRD and FESEM Characterisation

The as-prepared sulfur-doped powder X-ray diffraction (XRD) patterns are shown in Fig.-1A. X-ray diffraction (XRD) was used to examine the produced materials' crystalline structure and phase purity.

Both S-ZnO nanoparticles and the S-ZnO/Chitosan nanocomposite showed the same trends. Both samples' diffraction peaks exhibit a significant correlation with ZnO's hexagonal wurtzite structure, which is in line with the standard JCPDS-ICDD Card No. 01-080-0075. This demonstrates that crystalline ZnO with sulfur doping may be successfully synthesised without changing the basic crystal structure. The intensity of the distinctive ZnO diffraction peaks in Fig.-4 considerably rises when ZnO is incorporated into the chitosan matrix as opposed to pure ZnO-S nanoparticles. The successful creation of a heterostructure is shown by this increase in peak intensity, which implies enhanced crystallinity and a robust interaction between ZnO and chitosan. Subtle variations in peak form and intensity, which represent the hybrid character of the material, further corroborate the existence of chitosan in the composite. A closer look at the XRD pattern in Fig.-2A shows that ZnO-S exhibits a very weak peak at about 23° 2θ, which may be caused by residual Sulphur species or small crystalline or amorphous impurities. At roughly 32°, 35°, and 37° 2θ, strong and distinct peaks are seen; the peak at 37° has the maximum strength. These peaks further support the wurtzite structure by matching the (100), (002), and (101) crystal planes of hexagonal ZnO, respectively. The ZnO-S/chitosan nanocomposite in Fig.-5 has comparable peak positions at approximately 32°, 35°, and 37° 2θ, with the peak at 37° being the most pronounced. This indicates that the crystal structure of ZnO is maintained following chitosan incorporation. The JCPDS standard (01-080-0075) indexes additional diffraction peaks at 47° (102), 57° (110), 63° (103), and 68° (112) 2θ, which similarly correspond to higher-order reflections of hexagonal ZnO. Additionally, a peak is seen at 20° 2θ, which is explained by the distinctive diffraction of chitosan. This wide, low-intensity peak shows that the chitosan was successfully incorporated into the nanocomposite and is usually linked to its amorphous or semi-crystalline areas. Overall, the successful doping of Sulphur into ZnO while preserving its hexagonal wurtzite crystal structure is confirmed by the XRD investigation. Additionally, the addition of chitosan increases peak intensities rather than disrupting the ZnO crystalline lattice, suggesting better crystallinity and efficient composite synthesis. Maintaining ZnO's photocatalytic qualities while taking advantage of chitosan's synergistic benefits depends on this structural integrity.[11-13.]

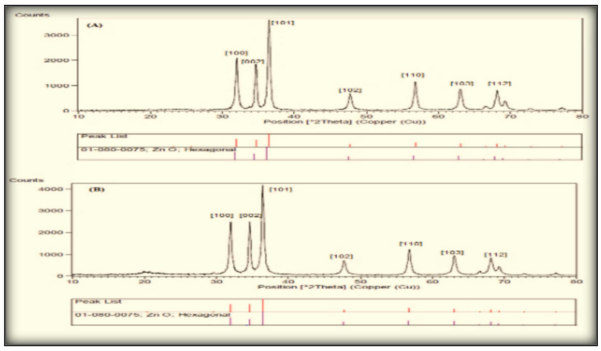

Fig.-4: XRD Spectrum for SUF -ZnO-S Nanoparticle

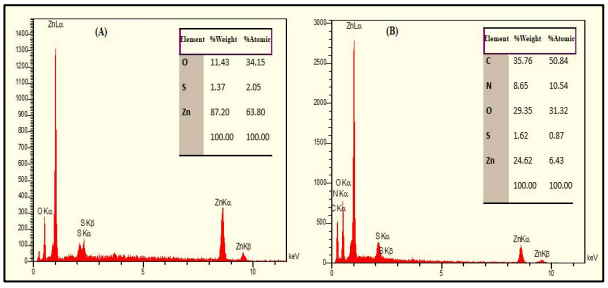

Fig.-5: FESEM Spectrum for SUF_ZnO-S Nanoparticle

Scanning Electron Microscope (SEM)

The shape and elemental content of the synthesised ZnO-S (sulfur-doped zinc oxide) and ZnO-S/Chitosan nanocomposite were investigated using Flame Emission Scanning Electron Microscopy (FESEM) and Energy-Dispersive X-ray Spectroscopy (EDX) (Fig.-6).

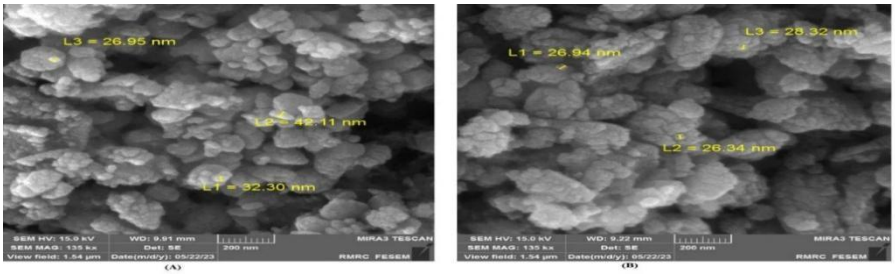

Fig.-6: SEM Images of SUF_ZnO-S Nanoparticle

Both materials have primarily spherical structures with diameters in the nanometer range, as shown by the FESEM micrographs.

Mechanism of Methyl Orange (MO) Dye Degradation

Methylene red dye degradation in an aqueous medium was used to assess the photocatalytic efficacy of SUF_ZnO-S nanoparticles. Precursor solutions with varying concentrations (100 g/mL, 200 g/mL, and 300 g/mL) were used to create ZnO-S nanoparticles. To achieve adsorption–desorption equilibrium, the suspensions were magnetically agitated for 30 minutes in the dark before being exposed to radiation. After that, the photocatalytic reactions were conducted in a typical photoreaction while exposed to UV light. Figure-7 (a–c) displays the time-dependent variation in the methylene red absorption spectra for reaction intervals of 0, 30, 60, 90, 120, and 150 minutes. Methylene red's distinctive absorption peak at 664 nm dramatically dropped within the first hour of exposure to UV light, then gradually reduced for up to four hours. Figure-9 shows the photocatalytic degradation efficiency of SUF-ZnO-S nanoparticles. With spectra acquired at 0, 15, 30, 45, 60, 75, and 90 minutes of UV exposure, 30 mg/100 mL showed the best degrading efficiency among the tested concentrations.

The photocatalytic degradation efficiency of the dye was calculated using the following equation:

$$\text{Percentage Photo-degradation} = C_0 - C/C_0 \times 100$$

In this case, CCC indicates the ultimate concentration following photo-irradiation, whereas C0C_0C0 represents the initial dye concentration. The decrease in dye concentration attests to ZnO-S's photocatalytic activity. Visual proof of nanoparticle-assisted degradation is provided by a drop in the absorption peak intensity as detected by UV–visible spectrophotometry.[14]

The complex process of dye degradation by the catalyst is influenced by both the energy source's intensity and the catalyst's intrinsic properties. More reactive species, such as hydroxyl radicals (•OH) and superoxide radicals (O_2 •$^-$), are generated on the surface of the nanoparticles since the inquiry uses UV light irradiation as the energy source. This successfully breaks down the Methyl Orange colouring. As seen in Fig. 18 and Equations, when the photocatalyst absorbs photons with energy equal to or greater than its band gap, an electron (e^-) is driven from the valence band (VB) to the conduction band (CB), leaving a hole (h^+) in the VB. The surface of the photocatalyst receives the electrons and holes created during photolysis. When the valence band holes (h^+) interact with H_2O, hydroxyl radicals (·OH) are produced. Efficient separation is crucial because recombination (e-h+→heat) reduces efficiency. When dissolved oxygen (O_2) combines with conduction band electrons (e^-) (·O_2^-), superoxide radicals are produced. After electrons are excited from the valence band to the conduction band, photogenerated electrons and holes migrate to the catalyst's surface. They interact with adsorbed species there through redox reactions. The generated superoxide and hydroxyl radicals attack Colour molecules through oxidation and reduction processes.

Table-1: Comparison of Degradation Efficiency of S-doped ZnO Nanomaterials using Selenicereus Undatus Peel Extract with Reported Works

S. No	Material	Dye	Time(min)	Source	Degradation(%)	Reference
1	Fe-NP using Trigonella foenum-graecum seed extract	MO dye	180 min	UV-light	71%	[15]
2	Zinc ferrite NP's	RhB dye	180 min	UV-light	82.1%	[16]

3	Zinc oxide nanomaterials	BG dye	120 min	UV-light	86.68%	[17]
4	ZIF-8	MB dye	720 min	UV-light	90%	[18]
5	TiO_2 nanoparticles	MO dye	120 min	UV-light	90.26%	[19]
6	Titania nanoparticles	MB dye	90 min	UV-light	79.5%	[20]
1	Co/TiO_2 nanoparticles	MO dye	90 min	UV-light	82.00%	[21]
2	ZnO + SnO_2 NP's	MO dye	90 min	UV-light	85.50%	[22]
3	Mn-doped ZnO nanoparticles	MB dye	150 min	UV-light	90.00%	[23]
4	Aqueous TiO2 suspensions	MO dye	90min	UV-light	82.50%	[24]
5	$Bi_2MoO_6/g\text{-}C_3N_4$	Organic pollutants	180 min	UV-light	90.50%	[25]
6	ZnO+Calotropis procera NP;s	MO dye	120 min	UV-light	88.00%	[26]
7	ZnO Dragon Fruit Extracts	MO dye	180 min	UV-light	82.00%	[27]
8	Ce-doped NiO nanoparticles	MB and Rh-B	120 min	UV-light	89.50%	[28]
9	Bi2MoO6/g-C3N4	Toxic org. poll.	180 min	UV-light	84.00%	[29]
10	CeO_2	MO dye	180 min	UV-light	71%	[30]
11	CeO_2	RhB	180 min	UV-light	82.1%	[31]
12	Mn doped ZnO/CSAC	BG dye	120 min	UV-light	86.68%	[32]
13	ZnO/CSAC	BG dye	120 min	UV-light	90.26%	[33]
14	ZnO Nanoparticles	None	90 min	UV-light	70%	[34]
14	ZnO/Graphene Oxide	Graphene Oxide	60 min	UV-light	80%	[35]
15	TiO_2 /Sulfur-Doped ZnO NP's	TiO_2	90 min	UV-light	85 %	[36]
16	S-doped ZnO Selenicereus undatus –NP's	MO dye	90 min	UV-light	92.4%	Current Study

$$S\text{-}ZnO + h\nu \longrightarrow S\text{-}ZnO\ (h^+ + e^-) \quad (1)$$
$$S\text{-}ZnO + h\nu \longrightarrow S\text{-}ZnO\ (h^+ + e^-) \quad (2)$$
$$H_2O + h^+ \longrightarrow \cdot OH \quad (3)$$
$$.OH + MO \longrightarrow \text{Degradation product} \quad (4)$$
$$O_2^- + MO \longrightarrow \text{Degradation product} \quad (5)$$

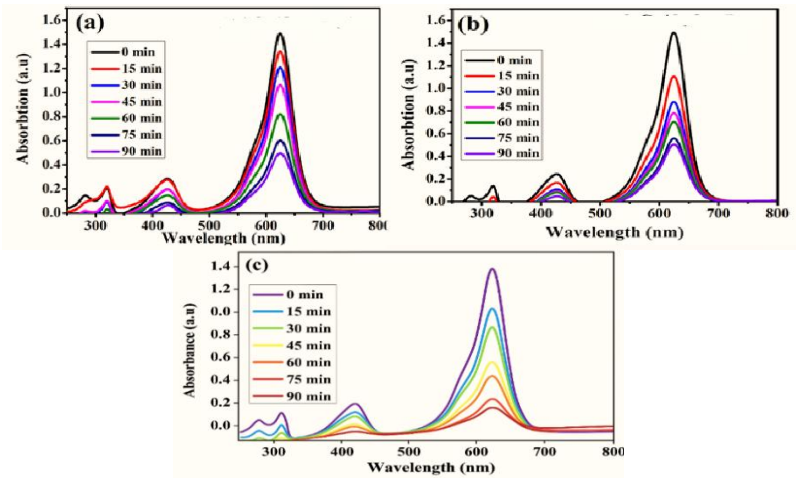

Fig.-7: Photo-Catalytic Efficiency of S-doped ZnO Nanomaterials (a) Dosage 10mg/100 mL (b) Dosage 20mg/100 mL and (c) Dosage 30mg/100 mL

CONCLUSION

When the valence band holes (h+) interact with H_2O, hydroxyl radicals (·OH) are produced. Efficient separation is crucial because recombination (e-h+→heat) reduces efficiency. When dissolved oxygen (O_2) combines with conduction band electrons (e^-) ($\cdot O_2^-$), superoxide radicals are produced. After electrons are excited from the valence band to the conduction band, photogenerated electrons and holes migrate to the catalyst's surface. They interact with adsorbed species there through redox reactions. The generated superoxide and hydroxyl radicals attack Colour molecules through oxidation and reduction processes. In particular, the S-ZnO catalyst retained outstanding stability during several reuse cycles and attained a

high degradation efficiency of Methyl Orange dye (up to 92.40%). All things considered, this green synthesis approach shows how tannery waste, dye industry waste, and chemical industry waste can be used as a sustainable resource to create high-performance photocatalysts. This method presents a viable route for extensive wastewater treatment applications, particularly for the elimination of artificial dyes. Future studies could examine the material's activity in visible light and evaluate its suitability for combating a wider variety of organic contaminants.

ACKNOWLEDGEMENTS

The authors sincerely appreciate the support and access to essential research facilities provided by the Research and Development Centre, Science and Humanities, Panimalar Engineering College (Autonomous), Chennai, India.

CONFLICT OF INTERESTS

The authors declare that there is no conflict of interest.

AUTHOR CONTRIBUTIONS

The present work is related to *SDG-6: Clean Water and Sanitation*. All the authors contributed significantly to this manuscript, participated in reviewing/editing and approved the final draft for publication. The research profile of the authors can be verified from their ORCID ids, given below:

A. Kistan https://orcid.org/0000-0003-1334-4331
P. Mahimairaj https://orcid.org/0000-0003-4063-2507
R. Jeevalatha https://orchid.org/000-0001-8071-8132
S. Mohan https://orcid.org/0000-0001-6538-3055
P. Sivakumar https://orcid.org/0000-0002-6009-3320

Cite this article as: A. Kistan *et al.*, *Rasayan J. Chem.*, 19(1), 575-582(2026), https://doi.org/10.31788/RJC.2026.1919577.

REFERENCES

1. K. Zahira, N. Aissaoui, D. Ismail, Julio A. Seijas, M. Vázquez-Tato, Nihel Klouche Khelil, and Noureddine Choukchou-Braham. *Molecules* **27,** 3439(2022), https://doi.org/10.3390/molecules27113439
2. M.S. Rao, T.B. Rao and C.P. Koteswara, *Rasayan Journal of Chemistry*, **13,** 1513(2020), http://dx.doi.org/10.31788/RJC.2020.1335799
3. N. Sarvaiya, H. Samata, S. Gulati and H. Patel, *Rasayan Journal of Chemistry*, **15(1)**, 564(2020), http://dx.doi.org/10.31788/RJC.2022.1516656
4. R.M. Mohareb, D.H. Fleita and O.K. Sakka, *Molecules,* **23**, 16(2011), https://doi.org/10.3390/molecules16010016
5. M. Sapnakumari, B. Narayana, B.K. Sarojini and L.N. Madhu, *Medicinal Chemistry Research*, **23**, 2368(2014), https://doi.org/10.1007/s00044-013-0835-6
6. H. Zhongshi, X.Wang, L.Ning, S. Fuqiang, and J. Zhou, *Bio resource Technology,* **377**, 128953 (2023), https://doi.org/10.1016/j.biortech.2023.128953
7. S. Momeni, and R.Ghorbani-Vaghei, *Scientific Reports*, **13**, 1627(2023), https://doi.org/10.1038/s41598-023-27940-6
8. T.L. Vijayakumar, P. Udhayakumar, and B. Balavairavan, *Polymer Engineering and Science*, **65**, 4070 (2025), https://doi.org/10.1002/pen.27271
9. A.N. Mayekar, H. Li, H.S. Yathirajan, B. Narayana and N.S. Kumari, *International Journal of Chemistry*, **2**, 114(2010), https://doi.org/10.5539/ijc.v2n2p114
10. V.Prasad, G. Gnanamani Simiyon, A. Elizabeth Mammen and N. Jayaprakash, *Rasayan Journal of Chemistry*, **12(2)**, 860(2019), http://dx.doi.org/10.31788/RJC.2019.1225226

11. S.Acharya and S.Dojalisa, *Rasayan Journal of Chemistry*, **16(4)**, 4(2023), http://doi.org/10.31788/RJC.2023.1648647
12. Irudayaraj, Auxilia Ruby Sagaya, Felicita Florence John, C. Divya Priya, R. Kanmani, and J. Amala Infant, *Zastita Materijala*, **66**, 90(2025), https://doi.org/10.62638/ZasMat1188
13. T. Tejeswara Rao and K. Naresh Kumar, *Recent Developments in the Synthesis and Applications of Pyridines*, **2023**, 605(2023), https://doi.org/10.1016/B978-0-323-91221-1.00005-1
14. Z. Benzarti, N. Joana, F. Pedro, S. Eduardo , C. Sandra and D. Susana, *Nanomaterials*, **15**, 991(2025), https://doi.org/10.3390/nano15130991
15. A. Zied, A. Hesham, A.M Beshr, H. Gomaa, YA. Mostafa, Y. Bahaa, M. Hayallah, and M. Abdel-Aziz, *Archiv der Pharmazie*, **356,** 2200464(2023), https://doi.org/10.1002/ardp.202200464
16. Thattil, Preeja and A. Leema Rose, *Rasayan Journal of Chemistry,* **13(2)**, 2(2020), http://dx.doi.org/10.31788/RJC.2020.1325558
17. T. Karnan, A. Stanly and S. Selvakumar, *Journal of Molecular Structure*, **1125**, 358(2016), https://doi.org/10.1016/j.molstruc.2016.07.029
18. S. Liao, S. Shibin, S. Minggui, R. Xiaoping, Si.Hongyan, J. Song and S. Zhanqian, *Bioorganic and Medicinal Chemical Letters,* **26,**1512(2016), https://doi.org/10.1016/j.bmcl.2016.02.024
19. R. Ibrahim Ali, H. Nazim, M. Ahmad Malik and K. Zaheer, *Journal of Photochem and Photobiology B: Biology,* **183**, 154(2018), https://doi.org/10.1016/j.jphotobiol.2018.04.014
20. F. Ajormal, F. Moradnia, S. Taghavi Fardood and A. Ramazani, *Journal of Chemical Reviewers*, **2**, 90(2020), 10.33945/SAMI/JCR.2020.2.2
21. R. Kumar, K. Girish, and U. Ahmad, *Nanoscience and Nanotechnology Letters*, **6,** 631(2014), https://doi.org/10.1166/nnl.2014.1879
22. J. Huan-Ping, C. Wang, Z. Yi-Wen, W. Peng and L. Ran, *RCS Advances*, **4**, 54454(2014), https://doi.org/10.1039/C4RA08820D
23. Li, Jingyi, M. Wanhong, C. Chuncheng, Z. Jincai, Z. Huaiyong and G. Xueping , *Journal of Molecular Catalysis A: Chemical*, **261**, 131(2007), https://doi.org/10.1016/j.molcata.2006.08.018
24. F. Azeez, E. Al-Hetlani, M. Arafa, Y. Abdelmonem, M. O. Amin and M. Metwally, *Scientific Reports*, **8**, 1(2018), https://doi.org/10.1038/s41598-018-25673-5
25. I. Ali, ML. Omar, Z. Alharbi, A. Alothman and A. Yacine Badjah, *Photochemistry and Photobiology*, **94**, 935(2018), http://dx.doi.org/10.1111/php.12937
26. S. Abbasi and M. Hasanpour. *Journal of Materials Science: Materials in Electronics,* **28(2)**, 1307(2017), https://doi.org/10.1007/s10854-016-5660-5
27. H. Yang, K. Zhang, R. Shi, X. Li, X. Dong and Y.Yu, *Journal of Alloys and Compounds*, **413**, 302(2006), https://doi.org/10.1016/j.jallcom.2005.06.061
28. V. Kanchana, S. Vasanthan, L. Mayavan and A. Kistan, *Journal of Electronic Materials*, **1**, 2122(2025), https://doi.org/10.1007/s11664-025-11739-4
29. V. V. Gawade, N. L. Gavade, S. B. Babar, A. N. Kadam and K. M. Garadkar, *Journal of Materials Science: Materials in Electronics,* **28**, 14033(2017), https://doi.org/10.1007/s10854-017-7254-2
30. D. Channei, B. Inceesungvorn, N. Wetchakun, S. Ukritnukun, N. Andrew, C. Jun and S. J. S. R. Phanichphant, *Scientific Reports*, **4**, 5757(2014), https://doi.org/10.1007/s10854-015-3823-4
31. K. Kaviyarasu, K. John, E. Manikandan, H. Mohamed and M. Maaza, *Scientific Reports*, **6,** 38064 (2016), https://doi.org/10.1039/C5RA16114B
32. R. Nithya, S. Ragupathy, D. Sakthi, V. Arun and N. Kannadasan, *Materials Research Express*, **7,** 075002(2020), 10.1088/2053-1591/aba025
33. E.L. Hashash, A. Maher and S. Shaban, *Synthetic Communications*, **49**, 630(2019), https://doi.org/10.1080/00397911.2019.1616096
34. H. Liu, M. Zhng and J. Li, Journal *of Hazard Materials,* **401**, 123456(2021), 10.1021/acsomega.0c03608
35. J. Kim, S. Park and H. Lee, *Applied Catalysis B: Environment and Energy,* **246**, 95(2019), 10.1016/j.jece.2021.105560

[RJC-9577/2026]